CHEMISTRY
A EUROPEAN JOURNAL

FULL PAPER

DOI: 10.1002/chem.201103433

Porous, Conductive Metal-Triazolates and Their Structural Elucidation by the Charge-Flipping Method

Felipe Gándara,[a] Fernando J. Uribe-Romo,[a] David K. Britt,[a] Hiroyasu Furukawa,[a] Liao Lei,[b] Rui Cheng,[c] Xiangfeng Duan,[b] Michael O'Keeffe,[a] and Omar M. Yaghi*[a, d, e, f]

Abstract: A new family of porous crystals was prepared by combining 1*H*-1,2,3-triazole and divalent metal ions (Mg, Mn, Fe, Co, Cu, and Zn) to give six isostructural metal-triazolates (termed MET-1 to 6). These materials are prepared as microcrystalline powders, which give intense X-ray diffraction lines. Without previous knowledge of the expected structure, it was possible to apply the newly developed charge-flipping method to solve the complex crystal structure of METs: all the metal ions are octahedrally coordinated to the nitrogen atoms of triazolate such that five metal centers are joined through bridging triazolate ions to form super-tetrahedral units that lie at the vertexes of a diamond-type structure. The variation in the size of metal ions across the series provides for precise control of pore apertures to a fraction of an Angstrom in the range 4.5 to 6.1 Å. MET frameworks have permanent porosity and display surface areas as high as some of the most porous zeolites, with one member of this family, MET-3, exhibiting significant electrical conductivity.

Keywords: charge flipping · electrical conductivity · metal-organic frameworks · porous materials · X-ray diffraction

Introduction

Metal–organic frameworks (MOFs) are porous crystals whose structures are constructed from metal-containing cationic units and anionic organic linkers.[1] Both components can be varied and functionalized for catalysis[2,3] and exceptional gas adsorption,[4–6] among many applications.[7–9] Thus far, MOFs with desirable porosity and stability are mostly made from organic links of carboxylates,[10,11] imidazolates,[12,13] and tetrazolates;[14,15] however, there is strikingly less work being reported on other linking functionalities.[16] We believe that a chief difficulty one encounters when embarking on making a new class of MOFs from previously undeveloped metal–linker chemistry is the tendency for the assembly reactions to yield microcrystalline powders rather than single-crystalline products. The latter are highly sought after because of the facility with which crystals of complex MOFs can be solved by using single-crystal X-ray diffraction techniques. Although structure-solution methods for powder X-ray diffraction (PXRD) data are used for solving the crystal structures of microcrystalline MOFs, these cases often require previous knowledge of the expected structure to achieve a satisfactory solution.[17] Unfortunately, when no previous knowledge is available for the expected structure, as is frequently the case in new metal-linker MOF chemistry, a potentially interesting MOF goes uncharacterized because of the challenges associated with obtaining their structure from powder X-ray diffraction techniques. Here, we demonstrate how the newly developed charge-flipping method is effective in solving the complex extended structures of metal triazolates (hereafter METs). These compounds, whose synthesis we describe below, are a new class of porous crystals that exhibit electronic conductivity and permanent porosity. Their structure could not be predicted easily due to the numerous ways in which the tridentate triazolate ligand can bind to the metal.

[a] Dr. F. Gándara, Dr. F. J. Uribe-Romo, Dr. D. K. Britt, Dr. H. Furukawa, Prof. M. O'Keeffe, Prof. O. M. Yaghi
Center for Reticular Chemistry
Department of Chemistry and Biochemistry
University of California, Los Angeles
Los Angeles, CA 90095 (USA)
E-mail: yaghi@berkeley.edu

[b] Dr. L. Lei, Prof. X. Duan
Department of Chemistry and Biochemistry
University of California, Los Angeles
Los Angeles, CA 90095 (USA)

[c] R. Cheng
Department of Materials Science and Engineering
University of California, Los Angeles
Los Angeles, CA 90095 (USA)

[d] Prof. O. M. Yaghi
NanoCentury. KAIST Institute
and Graduate School of EEWS (WCU) (Korea)

[e] Prof. O. M. Yaghi
Department of Chemistry, University of California
Berkeley, CA 94720 (USA)

[f] Prof. O. M. Yaghi
Molecular Foundry, Division of Materials Sciences
Lawrence Berkeley National Laboratory
Berkeley, CA 94720 (USA)

Supporting information for this article is available on the WWW under http://dx.doi.org/10.1002/chem.201103433.

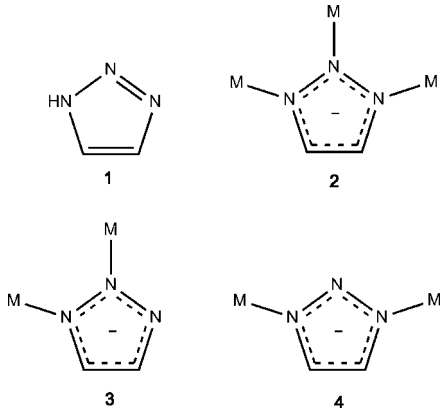

Scheme 1. The 1*H*-1,2,3-triazole molecule (**1**) deprotonates to form the triazolate anion, which is able to coordinate several metal atoms in different modes (**2**, **3**, and **4**).

The recent emergence of 1*H*-1,2,3-triazole (Scheme 1) as an object of click-chemistry and the ease with which it can be functionalized[18] coupled with its rich metal complexation modes[19–21] motivated us to take advantage of these favorable attributes and develop its framework chemistry by linking triazolate with metal ions. In particular (in contrast to imidazolates with four N atoms linked to the metal in tetrahedral coordination), in triazolates (with six N atoms per divalent metal), we expect six-fold (i.e., octahedral) coordination and a wider range of metals to form triazolates as indeed observed in the present study. We report the successful synthesis, structure elucidation from X-ray powder diffraction and charge-flipping method, and porosity of a family of six METs of divalent metals Mg, Mn, Fe, Co, Cu and Zn. We find that all the metal ions form the same MET framework (MET-1 to 6), in which the metal ions are octahedrally coordinated to triazolate. Five metal-centers are joined through six triply-bridging triazolate to form super-tetrahedral units, which lie at the vertices of a diamond-type structure. The variation in the size of metal ions across the series provides for precise control of pore apertures to a fraction of an Angstrom in the range 4.5 to 6.1 Å. We demonstrate that MET frameworks have permanent porosity and display surface areas as high as some of the most porous zeolites. In addition, we show that a member of this family, MET-3, exhibits significant electrical conductivity.

Results and Discussion

Crystalline MET materials ($M(C_2N_3H_2)_2$, M = Mg, Mn, Fe, Co, Cu, Zn) were obtained by solvothermal treatment of the metal salt (chloride or nitrate) and 1*H*-1,2,3-triazole. Full synthetic procedures can be found in the Supporting Information, section S1. The solid products were all insoluble in common organic solvents. Their FTIR spectra confirmed the absence of the N–H stretching modes at 3357 cm^{-1} in 1*H*-1,2,3-triazole and 3200 cm^{-1} in 2*H*-1,2,3-triazole,[22] which supports the bond formation between M^{II} and 1,2,3-triazolate to make extended structures of METs. This conclusion was further supported by the solid-state ^{13}C cross-polarization with magic-angle spinning (CP-MAS) NMR measurements, in which the spectrum for MET-6 displayed only one resonance signal at 128.8 ppm (130.3 ppm in triazole) for the triazolate carbon atoms. The equivalence of the carbon atoms indicates that the nitrogen atoms are all linked in the same way to the metal ions and that the triazolate ring must exhibit *mm*2 (C_{2v}) symmetry (see the Supporting Information, Figure S1).

Numerous attempts to obtain the METs as single crystals for X-ray diffraction were unsuccessful. Nevertheless, we were able to obtain all the METs as microcrystalline powders (Figure 1) exhibiting intense diffractions lines from

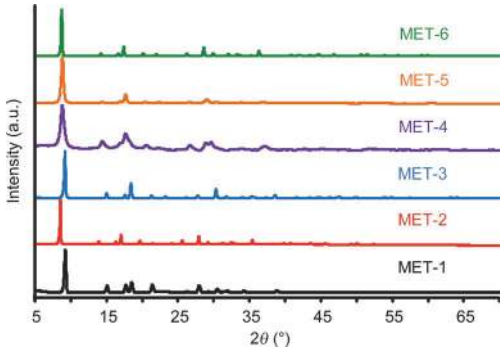

Figure 1. Powder X-ray diffraction patterns of MET-1 to 6.

which it was possible to determine accurate crystal structures (see the Supporting Information, sections S3 and S4). Here, we illustrate the structure elucidation for the MET-6 material, whose powder X-ray diffraction pattern contains reflections up to a resolution of 1.2 Å ($2\theta = 80°$ $Cu_{K\alpha}$ line). It was possible to index it ab initio using the Dicvol program,[23] resulting in a cubic unit cell with parameter $a = 17.67(1)$ Å (figures of merit $M_{20} = 30$, $F_{20} = 29$). The systematic absences suggested an *F*-centered cell, and potential space group $Fd\bar{3}$ or $Fd\bar{3}m$. With this information, a Pawley refinement was performed on the experimental diffractogram to obtain the integrated intensities (F^2_{obs} or I_{hkl}), resulting in convergent refinements and low residuals ($R_p = 2.48\%$, $wR_p = 3.49\%$). We then applied the charge-flipping algorithm with these extracted intensities and the refined unit cell parameters of MET-6 to calculate electron-density maps by using the Superflip program.[24] The charge-flipping method was developed recently[25,26] and it is gaining great acceptance within the crystallographic community for its effectiveness at solving complex structures. Some of these structures were determined by synchrotron PXRD data,[27] or in combination with electron-diffraction methods.[28] In the present case of METs, we show the applicability of this method for structure solution from powder data with the use of only common laboratory X-ray sources.

Since the chemical composition of the entire unit cell was unknown, we first used the obtained structure factors without any other chemical information and calculated rough electron density maps. From these early maps we were able to resolve the number and position of heavy atoms. The symmetry of these density maps is in agreement with the $Fd\bar{3}m$ space group. Two crystallographically independent Zn atoms can be located from the map at special positions $\bar{4}3m$ (0, 0, 0) and $3m$ (1/8, 1/8, 1/8).This disposition corresponds to an arrangement of the Zn atoms in a **dia** (diamond) net with a total of 24 Zn atoms per unit cell, with Zn atoms at the vertices and at the midpoints of edges of the net. Based on the composition of MET-6 as determined by elemental analysis, $Zn(C_2H_2N_3)_2$ (calcd (%): C 23.84, N 41.70, H 2.00; found: C 23.50, N 42.02, H 2.00), we determined that each unit cell contains $Zn_{24}C_{96}N_{144}H_{96}$. Further electron-density maps were calculated by using the algorithm adapted for powder patterns, in which histogram matching is performed by using the chemical composition of the unit cell (Figure 2a and 2b).[29]

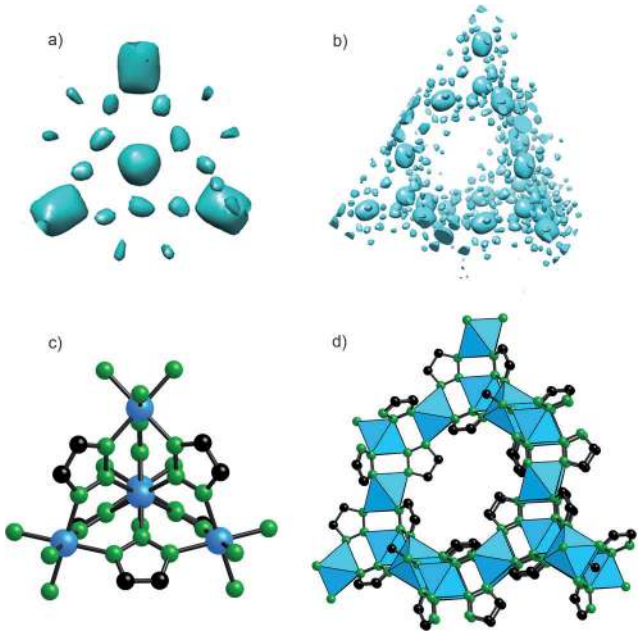

Figure 2. Electron density maps were generated by applying the charge-flipping method to PXRD data, clearly showing the position of the metal atoms and the triazole ring (a). The full unit cell is shown in (b). The crystal structure was refined accordingly. The tetrahedral SBU is shown in (c). The polyhedral representation of the framework is shown in (d). Metal atoms are represented as blue spheres (c) or polyhedra (d), nitrogen and carbon atoms are green and black spheres, respectively. Hydrogen atoms are omitted for clarity.

The second generation of electron-density maps resulted in higher resolution and showed the presence of 5-membered rings, which are attributed to the triazolate units (Figure 2a). Three of the atoms in these rings are adjacent to three different Zn atoms; chemical logic suggests that these three atoms are nitrogen. The 5-membered rings have a site-symmetry, $mm2$ (C_{2v}), which is consistent with the spectroscopic observations, with one of the N atoms at the (x, 0, 0) position, and the other two at (x, x, z) sites.

Additionally, these maps show the presence of a pore channel in which some electron density was observed, resulting from the presence of guest molecules (Figure 2b). To ensure the assignment of the space group and the symmetry derived from the density maps is not influenced by the initial choice of the space group for the extraction of the intensities, we expanded the intensities to $P1$ symmetry (equal partition of intensity of overlapped peaks), and then performed the charge-flipping algorithm followed by the symmetry search. Multiple runs all converged on the $Fd\bar{3}m$ space group. With the atomic positions derived from the electron-density maps with the best convergence residual, a crystal model was generated using Materials Studio;[30] Rietveld refinements[31] were performed over the experimental powder pattern obtaining convergent refinements with moderate residuals ($a=17.734(1)$ Å, $R_p=18.1\,\%$, $wR_p=25.1\,\%$, Figure 3). We attribute the value of these residuals

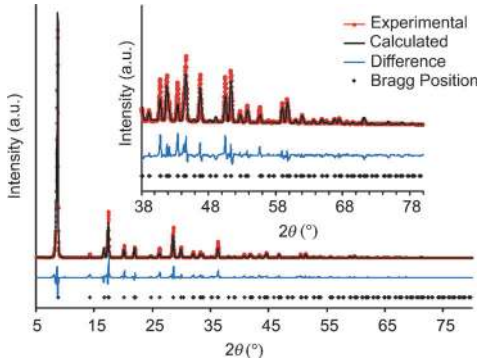

Figure 3. Rietveld refinement of the MET-6 compound showing the experimental (red), calculated (black) and difference (blue) patterns. Bragg positions are marked as black crosses. Inset: zoom of the high angle area.

to the effect of solvent disorder and guest molecules present inside the pore, as well as to the fact that we employed a conventional X-ray source with $K_{\alpha_{1,2}}$ contribution.

As an example for other METs, the X-ray crystal structure of MET-6 is illustrated in Figure 2. The Zn^{II} ions in the structure are all octahedral, bound to the N atoms of the triazolate rings. There are two independent Zn^{II} atoms, which are arranged forming a pentaatomic tetrahedral secondary building unit (SBU) (Figure 2c), with Zn atoms at the center and at the vertices of the tetrahedron. Each triazole ring bridges three Zn atoms: the N atom at position 2 binds to the atom at the center of the SBU, and the N atoms at positions 1 and 3 bind to two atoms at the vertices of the SBU. These tetrahedral units assemble by sharing vertices to form a **dia** network (Figure 2d).

The same protocol for the structure solution was carried out for MET-2, 3, and 5. In all the cases, the positions of the metal atoms were clearly identified in the electron-density maps. Rietveld refinements were equally performed, con-

verging with satisfactory residual values. In the case of MET-1 and 4, with much broader peaks, only a refinement of the unit cell parameters with full pattern profile matching could be performed (see the Supporting Information, section S3).

After we accomplished the structural solution of METs, the single-crystal structure of a Cd-triazolate with the equivalent atomic arrangement was independently reported,[32] which further supported the accuracy of our MET structure solution and adding yet another member to the family. However, no properties, such as porosity, and so on, were reported.

The calculated pore diameter varies in the MET series from 4.5 Å in MET-1 and MET-3 to 6.1 Å in MET-2. The values for the six MET materials are summarized in Table 1, together with their refined unit-cell volume and specific surface-area values. By choosing elements with different ionic radii, small changes in the lattice parameters are observed and networks with the same topology but different pore sizes are achieved (Figure 4).

All the METs are stable in air, since there were no significant changes in the PXRD patterns after several weeks of air exposure. They are also stable when immersed in common organic solvents (e.g., dichloromethane, chloroform, methanol, tetrahydrofurane, etc.), without any loss of crystallinity. The thermogravimetric analysis (TGA) indicate that the compounds are thermally stable, displaying no weight loss below the decomposition temperature, which varies with from approximately 250 °C in MET-5 to 400 °C in MET-2 (see the Supporting Information, section S5 for TGA data). The magnetic susceptibility measurement performed on MET-2 shows that this compound follows the Curie–Weiss law up to 5 K, with a Curie temperature of −21.9 K, and indicates that the Mn atoms are in high spin (calcd. $\mu_{eff}=5.8\ \mu_B$) (the Supporting Information, section S6).

The permanent porosity of the compounds was demonstrated by measurement of the N_2 adsorption isotherms at 77 K. All the MET compounds take up significant amounts of N_2 in the micropore region (Figure 5). The surface area of the METs was calculated according to the Brunauer–Emmet–Teller (BET) method[33] to give values varying from 370 to 890 $m^2 g^{-1}$ (450 to 1010 $m^2 g^{-1}$ for Langmuir surface areas), in which we chose the pressure range with values of $v(P_0–P)$ increasing with P/P_0 (v is adsorbed amount of N_2). These values are in good agreement with those geometric surface areas estimated from their crystal structures with the only exception of MET-5, probably due to an incomplete activation (see the Supporting Information, section S7). The step observed in the low pressure region of the MET-2 N_2 isotherm (also observed at lower relative pressure in the Ar isotherm, see the Supporting Information, section S7) can be attributed to a phase transition of the adsorbates[34] within the pores so that they can accommodate a higher number of gas molecules, resulting in the highest surface area among the series. The possibility of a structural change as the cause of the step should be ruled out by the absence of changes in the PXRD patterns of a sample evacuated to

Table 1. Comparison of the cell volume, pore size and surface area of the six MET materials.

MET-*n*	Metal	Cell volume [Å^3]	Void fraction [%]	Pore volume [cm^3 g^{-1}]	Cavity diameter [Å]	BET area [m^2 g^{-1}]	Langmuir area [m^2 g^{-1}]
MET-1	Mg	4533.9	22.4	0.18	4.50	430	510
MET-2	Mn	5971.7	40.5	0.35	6.12	890	1010
MET-3	Fe	4617.9	22.4	0.18	4.54	450	500
MET-4	Co	5215.8	35.3	0.26	5.16	600	760
MET-5	Cu	5322.2	24.0	0.15	4.86	370	450
MET-6	Zn	5577.9	25.3	0.17	5.06	460	480

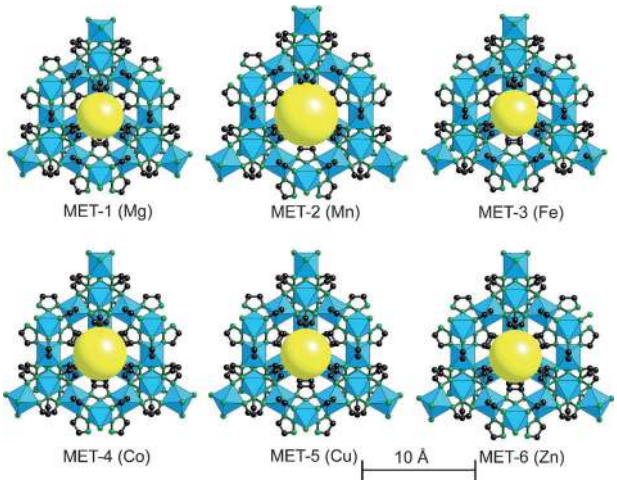

Figure 4. Illustration of the control of the pore size in the isostructural series of METs. Metal atoms are represented as blue spheres or polyhedra, nitrogen and carbon atoms are green and black spheres, respectively.

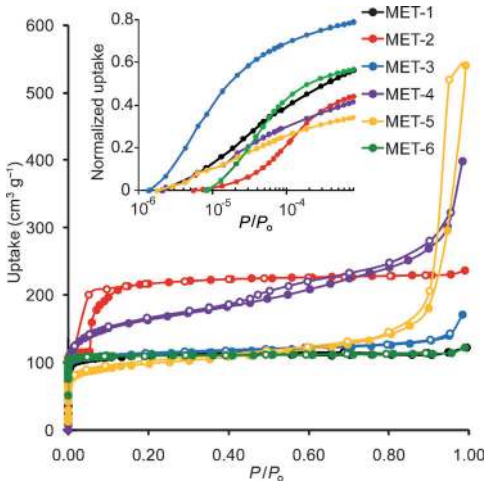

Figure 5. The six MET compounds have permanent porosity, as shown by the N_2 isotherm curves. Filled and open symbols represent adsorption and desorption branches, respectively. Inset figure: the normalized Ar isotherms are represented in a semi-logarithmic scale, to better appreciate the steps in the low pressure region, associated with the differences in the pore size.

a pressure below the step position and another sample evacuated and then filled with N_2 up to atmospheric pressure (the Supporting Information, section S7). The N_2 isotherms of MET-4 and 5 did not show a clear plateau region, which is attributed to the intergrain porosity because of the smaller crystal-size of both materials (as indicated by their broad PXRD diffraction peaks).

To confirm the differences in the pore sizes, we also measured the Ar adsorption isotherms at 87 K. Ar adsorption usually occurs at greater P/P_0 value compared to N_2, thus allowing observation of the differences in the low pressure range, which are associated with the differences in the pore sizes. The pressure range of micropore filling increases with an increase in pore diameter. At low pressures the differences in the uptake are associated with the pore size. For larger pore sizes, more pronounced steps appear at higher pressure. In the inset of Figure 5, the normalized Ar isotherms are plotted in a semi-logarithmic scale to better appreciate these differences. The trend observed is in good agreement with the one derived from the crystal data, in which MET-3 is the compound with the smallest pore size and MET-2 is the one with the largest pore, with intermediate values for the remaining compounds (Table 1).

Electrical conductivity is a property that remains relatively unexplored in the field of porous MOFs, despite the great interest that would be sparked by a multifunctional material with high surface area and electrical conductivity. We have performed preliminary tests on the electrical conductivity of MET-3. The small size and morphology of the crystals make them unsuitable for single-crystal measurements. Therefore, we performed the electrical measurements in a pressed pellet of the polycrystalline material. A conventional four-probe measurement was carried out with a pellet (1 cm in diameter and 0.5 mm in thickness) made from freshly prepared material. The results indicate that MET-3 is an intrinsically conducting material (Figure 6a), with a conductivity value of $0.77\times10^{-4}\,S\,cm^{-1}$.

There are very few studies in which a combination of electrical conductivity and porosity are reported. In 2009, Behera et al. reported a series of Prussian blue analogues with electrical conductivity.[35] One of them, prepared with Ru^{II}/Ru^{III}, shows a value of $5.7\times10^{-3}\,S\,cm^{-1}$ at 300 K, increasing to $1.9\times10^{-2}\,S\,cm^{-1}$ at 350 K. In 2010, the same group reported another microporous material prepared with a redox active dithiolane based ligand,[36] which reached $1\times10^{-4}\,S\,cm^{-1}$ only after exposure to I_2 vapor ($1\times10^{-8}\,S\,cm^{-1}$ for the as synthesized compound). Also in 2010, Zeng et al. reported a porous MOF[37] that exhibits electrical conductivity with values 3.4×10^{-3} to $1.7\times10^{-4}\,S\,cm^{-1}$ after being loaded with I_2. The conductivity is mainly attributed to the high loading of I_2 rather than to the framework itself.

The conducting characteristics of MET-3 can further be improved through a doping process (Figure 6b), in which the sample is exposed to I_2 vapor. After 40 min of exposure, the conductivity value increases to $1.0\times10^{-3}\,S\,cm^{-1}$. PXRD patterns show that the material remains unaltered after the pellet formation and exposure to I_2. A possible explanation

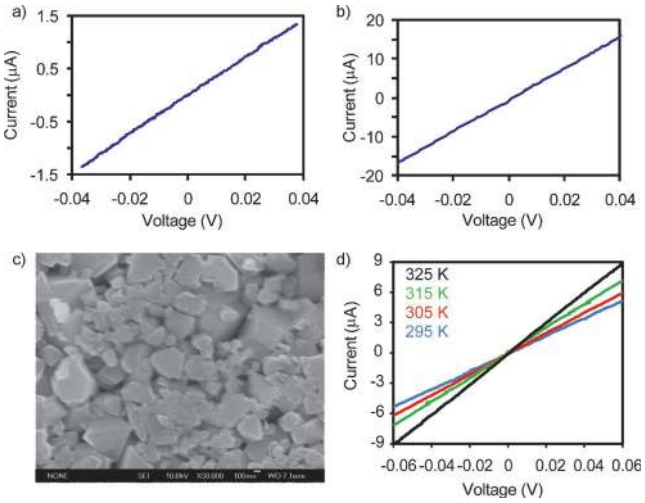

Figure 6. MET-3 is an intrinsically conducting material, as proved by the *I–V* curves recorded with the as synthesized (a) and I_2 doped (b) MET-3 pellets. (c) SEM image (30000×) of the MET-3 pellet employed for the conductivity measurements. (d) *I–V* curves recorded at different temperatures showing the increment in conductivity with the temperature.

for the large increase in conductivity on exposure to iodine is that Fe^{II} is being oxidized to Fe^{III}, resulting in mixed valence conductivity such is found in oxides like Fe_3O_4.

The electrical conducting characteristic of polycrystalline pellet materials may be largely limited by the existence of a large number of grain boundaries, as observed in the scanning electron microscopy (SEM) images of the pellet (Figure 6c). The conductivity measurements performed at different temperatures (Figure 6d) show an increment in the conductivity with the temperature. Due to the presence of boundaries and defects in the pellets, it seems feasible that boundary scattering dominates the electrical measurement, precluding from the observation of the intrinsic behavior of the material. With higher temperature, the kinetic energy of electrons increases. This will raise the probability of electron overcoming the boundary. Also, the thermal anneal will reduce the barrier height between the grain boundaries, resulting in an increased conductance. Nevertheless, this also indicates that the actual conductivity of the material should be higher than the one that can be extracted from the measurements performed with the pellets. With further development in the crystal growth process to allow formation of larger crystals, we expect that a more accurate characterization of the intrinsic electrical conductivity of these materials can be achieved. Additionally, we note that the sample is rather stable and the conductivity does not degrade with time, as indicated by the measurement of an undoped pellet left in air for eight weeks.

Experimental Section

Synthesis of METs: MET syntheses are exemplified here by the synthesis of MET-2; see section S1 in the Supporting Information for detailed syn-

thetic procedures for all METs. $Mn(NO_3)_2{\cdot}4H_2O$ (1 mmol) was dissolved in *N*,*N*-diethylformamide (DEF, 10 mL) in a vial. 1*H*-1,2,3-Triazole (2.5 mmol) was then added to this solution. The vial was capped and placed in a preheated oven at 120 °C for 24 h. After heating, a white solid formed, which was washed with DEF three times, and immersed in methanol for three days exchanging the solvent three times during this time. The solvent was removed by decantation and the solvent-wet powder was dried under vacuum (10^{-5} Torr) for 24 h at room temperature to afford a white powder, which was stored in a desiccator. Yield: 92% based on $Mn(NO_3)_2$. FTIR (KBr): $\tilde{\nu}$ = 3145 (m), 2938 (w), 2864 (w), 2656 (vw), 2515 (vw), 2414 (w), 2364 (w), 2195(w), 1719 (w), 1650 (m), 1456 (m), 1416 (m), 1381 (w), 1178 (s), 1098 (vs), 974(s), 798 (vs), 718 (w) cm^{-1}; elemental analysis calcd (%) for $Mn(C_2H_2N_3)_2$: C 25.13, N 43.98, H 2.12, Mn 28.77; found: C 24.95, N 41.89, H 2.05.

Powder X-ray diffraction measurements: Powder X-ray diffraction data were collected using a Bruker D8-advance θ–θ diffractometer in reflectance Bragg–Brentano geometry employing Ni-filtered $Cu_{K\alpha}$ line focused radiation at 1600 W (40 kV, 40 mA) power and equipped with a Vantec detector, with an electronic window of 6°. Samples were mounted on zero-background sample holders by dropping powders from a wide-blade spatula and then levelling the sample with a razor blade. The best counting statistics were achieved by collecting samples using a 0.02° 2θ step scan from 1–80° with exposure time of 10 s per step. All measurements were performed at room temperature and atmospheric pressure.

Gas-sorption measurements: All gas-adsorption experiments were performed on an Autosorb-1 automatic volumetric gas adsorption analyzer (Quantachrome, Boynton Beach, FL).

Scanning electron microscopy: Samples were measured by dispersing the material onto a sticky carbon surface attached to a flat aluminum sample holder. The samples were then gold-coated by using a Hummer 6.2 Sputter at ambient temperature and a pressure of 70 mTorr in an argon atmosphere for 30 s while maintaining a current of 15 mA. Samples were analyzed using a JOEL JSM-6700 scanning electron microscope using both the SEI and LEI detectors with an accelerating voltage of 7 kV.

Thermal gravimetric analysis: All samples were run on a Q-500 series thermal gravimetric analyzer (TA Instruments, New Castle, DE) with samples held in platinum pans in a continuous-flow nitrogen atmosphere. Samples were heated at a constant rate of 5 °C min^{-1} during all TGA experiments.

Electrical conductivity measurements: For the determination of the specific resistivity of the materials, the four-point probe DC measurement was used to eliminate the effect of contact resistance. The materials have been pressed as a bulk. 500 μm gold electrodes were thermally deposited by shadow mask on the bulk. The distance between electrodes is 1.6 mm. Finally, the four probe measurements were carried out directly after deposition using a Lake Shore TTP4 station under vacuum conditions and at different temperatures (295, 305, 315, and 325 K).

Acknowledgements

This work was sponsored by the U.S. Department of Energy (DE-FG02-08ER15935) and BASF SE (Ludwigshafen, Germany). We thank Prof. K. Barry Sharpless and Prof. Jason Hein for donation of raw materials. F.G. acknowledges funding by the Spain Ministry of Education through the "Programa de Movilidad de Recursos Humanos del Plan Nacional de I-D+i 2008–2011". O.M.Y. acknowledges support of WCU (EEWS), Korea.

[1] J. R. Long, O. M. Yaghi, *Chem. Soc. Rev.* **2009**, *38*, 1213–1214.
[2] A. Phan, A. U. Czaja, F. Gándara, C. B. Knobler, O. M. Yaghi, *Inorg. Chem.* **2011**, *50*, 7388–7390.
[3] S. J. Garibay, Z. Wang, S. M. Cohen, *Inorg. Chem.* **2010**, *49*, 8086–8091.
[4] H. Furukawa, N. Ko, Y. B. Go, N. Aratani, S. B. Choi, E. Choi, A. Ö. Yazaydin, R. Q. Snurr, M. O'Keeffe, J. Kim, O. M. Yaghi, *Science* **2010**, *329*, 424–428.
[5] O. K. Farha, A. Ö. Yazaydin, I. Eryazici, C. D. Malliakas, B. G. Hauser, M. G. Kanatzidis, S. T. Nguyen, R. Q. Snurr, J. T. Hupp, *Nat. Chem.* **2010**, *2*, 944–948.
[6] Y. E. Cheon, M. P. Suh, *Angew. Chem.* **2009**, *121*, 2943–2947; *Angew. Chem. Int. Ed.* **2009**, *48*, 2899–2903.
[7] U. Mueller, M. Schubert, F. Teich, H. Puetter, K. Schierle-Arndt, J. Pastre, *J. Mater. Chem.* **2006**, *16*, 626–636.
[8] K. Kim, M. Banerjee, M. Yoon, S. Das, in Functional Metal-Organic Frameworks: Gas Storage, Separation and Catalysis, Vol. 293 (Ed.: M. Schroder), pp. 115.
[9] Y. Takashima, V. Martinez Martinez, S. Furukawa, M. Kondo, S. Shimomura, H. Uehara, M. Nakahama, K. Sugimoto, S. Kitagawa, *Nat. Commun.* **2011**, *2*, 168.
[10] D. J. Tranchemontagne, J. L. Mendoza-Cortes, M. O'Keeffe, O. M. Yaghi, *Chem. Soc. Rev.* **2009**, *38*, 1257–1283.
[11] M. Eddaoudi, H. Li, O. M. Yaghi, *J. Am. Chem. Soc.* **2000**, *122*, 1391–1397.
[12] K. S. Park, Z. Ni, A. P. Côté, J. Y. Choi, R. Huang, F. J. Uribe-Romo, H. K. Chae, M. O'Keeffe, O. M. Yaghi, *Proc. Natl. Acad. Sci. USA* **2006**, *103*, 10186–10191.
[13] A. Phan, C. J. Doonan, F. J. Uribe-Romo, C. B. Knobler, M. O'Keeffe, O. M. Yaghi, *Acc. Chem. Res.* **2009**, *42*, 58–67.
[14] M. Dincă, A. F. Yu, J. R. Long, *J. Am. Chem. Soc.* **2006**, *128*, 8904–8913.
[15] A. Maspero, S. Galli, V. Colombo, G. Peli, N. Masciocchi, S. Stagni, E. Barea, J. A. R. Navarro, *Inorg. Chim. Acta* **2009**, *362*, 4340–4346.
[16] a) G. Férey, C. Mellot-Draznieks, C. Serre, F. Millange, J. Dutour, S. Surble, I. Margiolaki, *Science* **2005**, *309*, 2040–2042; b) S. Galli, N. Masciocchi, V. Colombo, A. Maspero, G. Palmisano, F. J. Lopez-Garzon, M. Domingo-Garcia, I. Fernandez-Morales, E. Barea, J. A. R. Navarro, *Chem. Mater.* **2010**, *22*, 1664–1672.
[17] G. K. H. Shimizu, R. Vaidhyanathan, J. M. Taylor, *Chem. Soc. Rev.* **2009**, *38*, 1430–1449.
[18] J. Kalisiak, K. B. Sharpless, V. V. Fokin, *Org. Lett.* **2008**, *10*, 3171–3174.
[19] H. Duan, S. Sengupta, J. L. Petersen, N. G. Akhmedov, X. Shi, *J. Am. Chem. Soc.* **2009**, *131*, 12100–12102.
[20] K. S. Singh, K. A. Kreisel, G. P. A. Yap, M. R. Kollipara, *J. Organomet. Chem.* **2006**, *691*, 3509–3518.
[21] a) J. Chuang, W. Ouellette, J. Zubieta, *Inorg. Chim. Acta* **2008**, *361*, 2357–2364; b) S. Biswas, M. Grzywa, H. P. Nayek, S. Dehnen, I. Senkovska, S. Kaskel, D. Volkmer, *Dalton Trans.* **2009**, 6487–6495; c) D. Denysenko, M. Grzywa, M. Tonigold, B. Streppel, I. Krkljus, M. Hirscher, E. Mugnaioli, U. Kolb, J. Hanss, D. Volkmer, *Chem. Eur. J.* **2011**, *17*, 1837–1848.
[22] F. Billes, H. Endredi, G. Keresztury, *J. Mol. Struct.* **2000**, *530*, 183–200.
[23] A. Boultif, D. Louer, *J. Appl. Crystallogr.* **2004**, *37*, 724–731.
[24] L. Palatinus, G. Chapuis, *J. Appl. Crystallogr.* **2007**, *40*, 786–790.
[25] G. Oszlányi, A. Sütő, *Acta Crystallogr. Sect. A* **2004**, *60*, 134–141.
[26] G. Oszlányi, A. Sütő, *Acta Crystallogr. Sect. A* **2008**, *64*, 123–134.
[27] C. Baerlocher, F. Gramm, L. Massueger, L. B. McCusker, Z. He, S. Hovmoeller, X. Zou, *Science* **2007**, *315*, 1113–1116.
[28] J. Sun, C. Bonneau, A. Cantin, A. Corma, M. J. Diaz-Cabanas, M. Moliner, D. Zhang, M. Li, X. Zou, *Nature* **2009**, *458*, 1154–1158.
[29] C. Baerlocher, L. B. McCusker, L. Palatinus, *Z. Kristallogr.* **2007**, *222*, 47–53.
[30] Materials Studio v 5.0.0.0, **2009**, Accelrys Software Inc.
[31] R. A. Young in *The Rietveld Method*, IUCr Book Serials, Oxford University Press, Oxford, **1993**.
[32] H. Zhou, Y.-H. Peng, X.-D. Du, J.-L. Zuo, X.-Z. You, *CrystEngComm* **2009**, *11*, 1964–1970.
[33] K. S. Walton, R. Q. Snurr, *J. Am. Chem. Soc.* **2007**, *129*, 8552–8556.
[34] Rouquerol F, Rouquerol J, Sing K in *Adsorption by powders and porous solids: principles, methodology and applications*, Academic Press, San Diego, CA, **1998**.

[35] J. N. Behera, D. M. D'Alessandro, N. Soheilnia, J. R. Long, *Chem. Mater.* **2009**, *21*, 1922–1926.
[36] Y. Kobayashi, B. Jacobs, M. D. Allendorf, J. R. Long, *Chem. Mater.* **2010**, *22*, 4120–4122.
[37] M.-H. Zeng, Q.-X. Wang, Y.-X. Tan, S. Hu, H.-X. Zhao, L.-S. Long, M. Kurmoo, *J. Am. Chem. Soc.* **2010**, *132*, 2561–2563.

Received: November 11, 2011
Published online: June 22, 2012

